Patterning of NiCr(80/20) on Al$_2$O$_3$ Using Picosecond Laser Pulses

Oliver SUTTMANN*, Jan F. DUESING*, Ulrich KLUG* and Rainer KLING*

Laser Zentrum Hannover e.V., Hollerithallee 8, 30419 Hannover, Germany
E-mail: o.suttmann@lzh.de

This paper concentrates on the characterisation of the ablation process of thin strain sensitive NiCr films deposited on Al$_2$O$_3$ substrates. The optical skin depth of NiCr (80/20) is identified. Removal experiments with single and multiple pulse point ablations are carried out on Al$_2$O$_3$ bulk substrates with different NiCr thicknesses. The experiments reveal the maximum NiCr film thickness for single pulse ablation. NiCr films with a higher thickness have to be processed in a multiple pulse processing strategy. Calculation of the beam radii using Liu plots revealed radii larger than the actual measured beam radius. The radius increase has been identified to consist of two parameters, one representing a special jitter of the experimental setup used, and a second thickness dependent parameter.

Keywords: laser ablation, patterning, incubation model, strain gauge

1. Introduction

1.1 State-of-the-art Strain Gauges

Strain measurement using strain gauges in industry and research is an important task for many scientific and industrial applications. Strain gauges are in most cases piezoresistive sensors; electrical conductors changing their electrical resistance when strained.

The most common strain gauges today are foil strain gauges consisting of a flexible polymer foil with a strain sensitive conductive path on top. Strain measurement of components requires application of the foil strain gauge usng adhesives. The adhesives used are a major limiting factor regarding the environmental conditions and longtime stability. Changes in humidity and temperature cause decrease of sensor performance. Even long term mediate temperatures approximately 100°C to 200°C lead to problems concerning reliable strain measurement, although sensing materials such as constantan or NiCr could work up to much higher temperatures [1].

One approach to overcome the limitations of the adhesives is the use of sputtered thin film strain gauges. Thin film strain gauges consist of sensing and isolation layers directly deposited onto the target to be measured. The sensor geometry is patterned afterwards by means of photolithography. Early thin film strain gauges have been developed by Gregory, Lei and Lüthje [2-4]. These new sensors could overcome limitations based on the adhesives used before and opened up new applications, e.g. strain measurement on turbine blades. Thin film sensors are today mostly applied when measuring injection pressure in modern combustion engines.

Nevertheless, photolithographically patterned strain gauges suffer from two big disadvantages: (i) the need for sensor trimming and (ii) the restriction to flat or nearly flat surfaces, due to the lithography masks.

Using laser ablation for the patterning and trimming seems to be a promising method to overcome the drawbacks of photolithography, and furthermore to reduce the manufactoring costs for low or medium lot size production.

Applying thin films on three-dimensional surfaces for sensor manufactoring will lead to inhomogeneous film thicknesses for both the sensing layer and the isolation layer. Thus the patterning process to be developed has to be robust against variations in both sensor and isolation film thickness.

This paper focuses on the removal behavior of metal thin films (sensing layer) and Al$_2$O$_3$ films (isolation layer). The sensor layer is chosen to be NiCr with a composition ratio of 80 weight percent nickel and 20 weight percent chromium. This alloy shows a low temperature coefficient of resistance, and therefore is well suited for strain sensors. Al$_2$O$_3$ is an established isolator and can be deposited with good reproducibility using standard PVD processes.

1.2 Thin Film Laser Ablation

Thin film laser ablation has been investigated thoroughly for pure metals and different pulse durations [5]-[9]. As far as the authors know NiCr alloys have not been investigated by other research groups. Based on our first results from recent experiments on patterning NiCr [10] we can state the following conclusions: (i) the ablation width depends on the applied fluence for non-uniform energy distributions. (ii) The ablation threshold decreases with an increasing number of repetitions (incubation effect). (iii) The ablation threshold depends on the film thickness. In this work we refine the experimental data a detailed discussion of the ablation behavior.

The correlation between energy per pulse and the diameter of the affected area has been identified first by Liu [5] and has been frequently used thereafter. Ablation will only take place, if the local fluence H is higher than the ablation threshold H_{thresh}. In the case of Gaussian energy distribution, given by

$$H(r) = H_{max}e^{-2\left(\frac{r}{\omega_0}\right)^2}$$

(1)

with radial position r and spot radius ω_0 the correlation between ablation diameter D and applied fluence H can be described as

$$D^2(H) = 2\omega_0^2 \, ln\left(\frac{H}{H_{thresh}}\right). \tag{2}$$

This behavior can be observed for each pulsed laser system. This knowledge can be used to determine the exact ablation threshold and beam diameter experimentally on the work piece. Furthermore, this behavior can be applied to other occurring phenomena like melting, evaporation or laser induced periodic surface structures (LIPSS)[5].

Energy deposited into the work piece below the ablation threshold still can affect the material. This deposited energy may lead to formation of the ablation threshold for trailing irradiations. This effect is called the incubation effect and was identified first by Jee [5]. The incubation effect for metals can be described as

$$H_{thresh}(n) = H_{thresh}(1)n^{S-1} \tag{3}$$

with number of pulses n, single pulse ablation threshold $H_{thresh}(1)$ and incubation factor S. Incubation factors below one describe a decrease of the ablation threshold with an increasing number of irradiations. Values of S above one describe an increasing ablation threshold with an increasing number of irradiations. No change of the ablation threshold with an increasing number of irradiations is described by an incubation factor of one. The incubation factor S can also be determined by plotting the accumulated fluence nH

$$nH_{thresh} = H_{thresh}(1)n^S. \tag{4}$$

Although equations (3) and (4) describe a mathematically identical relation, calculation of the incubation factor by least square fits might lead to different results. Thus it should be stated which equation has been used to determine the incubation coefficient S. The incubation effect has been reported for pulse durations in the nanosecond and femtosecond pulse duration regime [5],[7].

The dependency of ablation thresholds on the film thickness has been investigated by Güdde, Hohlfeld and Siegel [7]. They detected increasing ablation thresholds with increasing film thickness up to a certain critical film thickness. Ablation threshold stays constant for films with thicknesses above this threshold thickness. This mainly thickness depends on two factors: (i) the material and (ii) the pulse duration used for the experiments. In the case of nanosecond laser pulses the elements Ni and Cr as pure metals show an increase of the thresholds for melting and vaporization until the film thickness exceeds thermal diffusion length L_{thresh}. The thermal diffusion length can be calculated by the expression

$$L_{thresh} = \sqrt{\frac{2K\tau}{C}} \tag{5}$$

with thermal conductivity K, pulse duration τ and specific heat capacity C. For the investigated pulse duration, Ni shows a thermal diffusion length of about 700 nm, while Cr shows a slightly higher thermal diffusion length of $L_{thresh}>1000$ nm. These values are in good agreement with the determined threshold thickness determined by Siegel [9].

When applying pulses with duration in the femtosecond range, the threshold thickness for Ni is about 50 nm and Au

shows a threshold of approximately 700 nm. This value is much larger than expected from equation (5), and much higher than the optical skin depth. Irradiation with pulses in the ultra short pulse duration regime leads to two different temperatures for the electrons and the lattice. This behavior has been described in the two temperature model [11]. The heated electrons transport energy by diffusion or ballistic effects into the depth of the material, until relaxation occurs between the electron system and the lattice [12]. The electron diffusion length L_e has been identified as the major energy transport mechanism. The diffusion electron diffusion length L_e is dependent on the electron-phonon coupling constant g. The dependence can be described by the mathematical expression $L_e \propto g^{-1/2}$. Calculation of L_e requires the knowledge of the electron-phonon coupling constant g and other physical properties such as the thermal conductivity of the electron system. The required properties can only be determined for each material with high experimental effort. This is the reason why these properties are only known for a small number of pure elements.

Ni shows a coupling constant of $36*10^{16}$ Wm^{-3}K^{-1} and Au as another example shows a coupling constant of $2.1*10^{16}$ Wm^{-3}K^{-1}. Calculations published in [8] show that the electron diffusion length L_e correlates with the film thicknesses, up to which damage and removal thresholds depend on the film thickness, for Ni and Au. This film thickness is called critical film thickness. Cr shows a coupling constant of $42*10^{16}$ Wm^{-3}K^{-1}. The critical film thickness of Cr for ultra-short laser pulses is not known as far as the authors know. The coupling constant g emphasizes the threshold depth for Cr being in the same range as for Ni.

The aforementioned phenomena like the correlation between fluence and ablation diameter, the incubation model and the energy diffusion have not been published for the chosen sensor film NiCr (80/20). This paper presents results of experiments to estimate the impact of the aforementioned effects on laser structuring parameters for successful fabrication of NiCr strain gauges on three-dimensional surfaces.

2. Experimental

The experiments are executed with a commercially available Nd:YVO$_4$ laser in MOPA design with a pulse duration
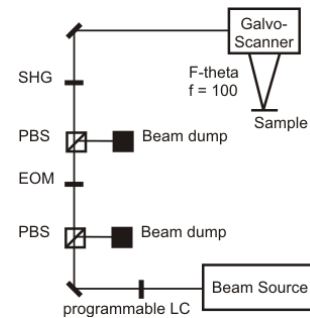
Fig. 1 Experimental setup

of 15 ps (LUMERA LASER RAPID). The wavelength is chosen to be 532 nm. This wavelength is a compromise between small spot size and high power loss due to harmonic generation.

An electro-optical modulator is used as an external shutter to run the laser in a quasi-stationary mode and provide constant pulse energy from the first pulse applied to the work

piece. Relative movement between sample and laser focus is realized by a galvo scanner. Focusing is performed using an f-theta lens with a focal length of 100 mm. The experimental setup is depicted in Fig. 1.
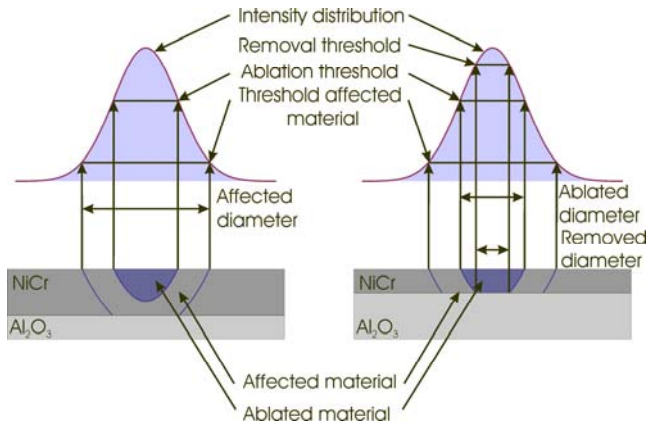
Fig. 2 Comparison affected, ablated and removed diameter

The patterning of strain gauges requires a full galvanic isolation of the sensor from the rest of the work piece. The ablation depths per pulse have been previously determined for nickel by other researchers. Typical ablation depths are smaller than 50 nm [12]. Thus, metal films with thicknesses which are investigated in this work are not expected to be entirely ablated with single pulses as depicted in Fig. 2. For this reason, the experiments published here do not aim at the ablation threshold but at the removal threshold, which is characterized by complete removal of the NiCr film. The removal thresholds are expected to be higher than the ablation thresholds.
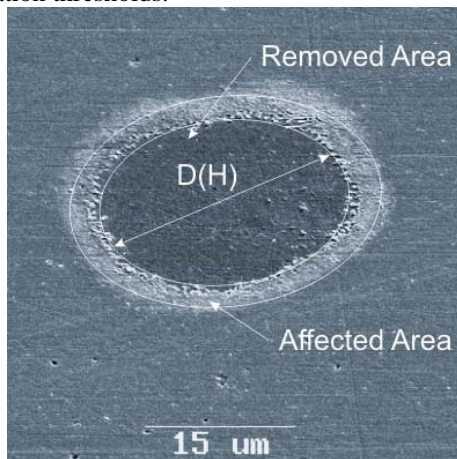
Fig. 3 SEM picture of a spot irradiated with n=100 pulses, fluence H=0.48 J/cm² and NiCr film thickness of 100 nm. Removed diameter $D(H)$ is highlighted as well as an affected diameter. The Al$_2$O$_3$ substrate shows no ablation marks. The angle of view is 45°.

The aim of the experiments is (i) to verify the dependency of the diameter of the material removed on the fluence, (ii) to determine the removal threshold as a function of the number of pulses and film thickness and (iii) to create a basis for the parameter used for line ablations.

For the creation of single shot ablations, lines are scanned with a scanning speed sufficient to ensure separation of ablations created by trailing pulses. Multiple shot ablations are performed by passing the same line several

times. Scanner and laser pulses are synchronized to ensure that the pulses always hit the same point on the samples within an accuracy of approximately one to two µm when passing multiple times. The effective line frequency resulting from scanning speed and scanning length is 100 Hz. Heating of the metal thin film due to residual heat can be neglected in this case, because the applied pulse repetition rate of 100 Hz is much lower than previously determined repetition rates leading to melting by residual heat. The negligible amount of molten material as seen in Fig. 3 underlines this assumption. Ablation with repetition rates in the high MHz regime will lead to an increase of molten material. The same effect will occur when applying pulse durations in the nanosecond regime.

The number of irradiations is varied from 1 to 1000 pulses. The beam radius is measured with a Micro Spot Monitor (MSM) and determined to be 11.5 µm. The energy per pulse is varied in the range from 0.15 µJ up to 4.3 µJ, resulting in fluences from 60.2 mJ/cm² to 1.73 J/cm². Fluence levels are increased by a factor of 1.3 starting from the lowest level in order to provide equidistant values on a logarithmic scale.

3. Results and Discussion

The optical skin depth of NiCr is determined by a Perkin Elmer Lambda 900 spectrometer. For that purpose transmission measurements of NiCr films sputtered on clear glass substrates have been performed. The film thicknesses of 23nm, 51nm and 78 nm have been used. Transmission of thicker films was too low to ensure exact measurement. The absorption in the glass substrate and the reflection on the thin film surface are assumed to be constant. The optical skin depth is calculated using the Beer-Lambert law

$$I(z) = I_0 e^{-\alpha z} = I_0 e^{-\frac{z}{\delta}} \tag{10}$$

with z the penetration depth, I_0 the absorbed intensity, $I_{trans}(z)$ the light transmitted to depth z and the absorption coefficient α and optical skin depth δ. The determined skin depth and the values of Ni and Cr as pure metals are depicted in Table 1.

Table 1: Optical skin depth for λ=532 nm

Material	Optical skin depth
NiCr (80/20)[1]	12.9±1.4nm
Ni[2]	13.4nm
Cr[2]	9.5nm

[1] based on own measurements
[2] interpolated from [13]

The removed spot diameters are measured and averaged for each film thickness. Due to the Gaussian intensity distribution the influence of the fluence on the squared ablation diameter can be stated by equation (2). The removed diameters are fit to the function

$$D^2 = a\ln(H) + b \tag{9}$$

in order to calculate the removal threshold and the effective beam radius. Only data with more than five valid

removal diameters are taken into account for the determination of the removal threshold to minimize errors. An exemplary plot for one film thickness is depicted in Fig. 4.
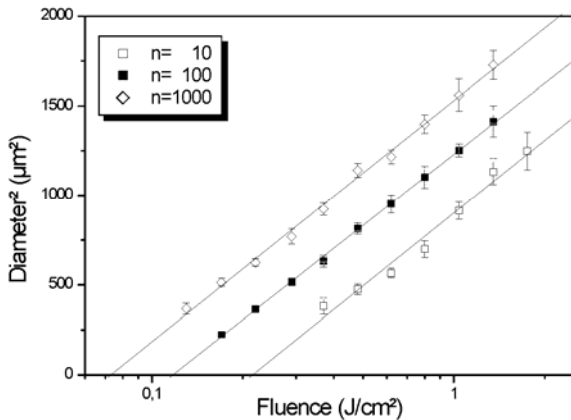
Fig. 4 Exemplary Liu plot for NiCr 51 nm film thickness

The removed diameter squared is depicted as a function of the fluence for exemplary number of irradiations. The error bars represent the standard deviation of each squared diameter. Solid lines represent the fit functions determined using equations (2) and (9). The plot shows good linearity for all depicted numbers of irradiation. Spots with less than ten irradiations did not provide five or more data points and are consequently neglected to minimize errors when fitting. Hence, only removal thresholds at least five fluence levels below the maximum achievable fluence can be determined.

The diameter squared plot shows that the removal of metallic thin films can be described with the plots suggested by Liu.
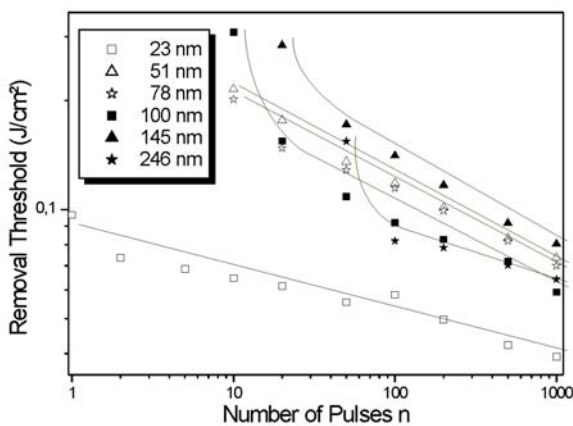
Fig. 5 Removal thresholds determined by Liu plots

To determine the removal thresholds for all different film thicknesses, this regression analysis is performed for each data point depicted in Fig. 5 representing a different number of pulses. The removal thresholds decrease with increasing number of pulses for all NiCr film thicknesses. Film thicknesses above 23 nm do not allow determination of removal thresholds for low numbers of pulses, when applying the condition of at least five valid data points. Thus, incubation coefficients cannot be determined for these film thicknesses. Nevertheless, it is obvious that the

incubation coefficient S as introduced in equation (3) and (4) has to be smaller than one.

The film with a thickness of 23 nm exhibits significantly lower removal thresholds than the other films. This is the only film thickness which allows for plotting removal threshold determined from Liu plots over the full range of repetitions. The removal thresholds of thicker films do not increase significantly.

In order to test the validity of the incubation effect for removal, the removal thresholds for low numbers of pulses have to be determined. This is realized by using visual backlight microscopy examination of ablated spots. This method allows for the determination of removal thresholds by identification of fluence and the number of pulses which lead to complete film removal, without the need of at least five fluence levels above the removal threshold, as in the case of Liu plots.
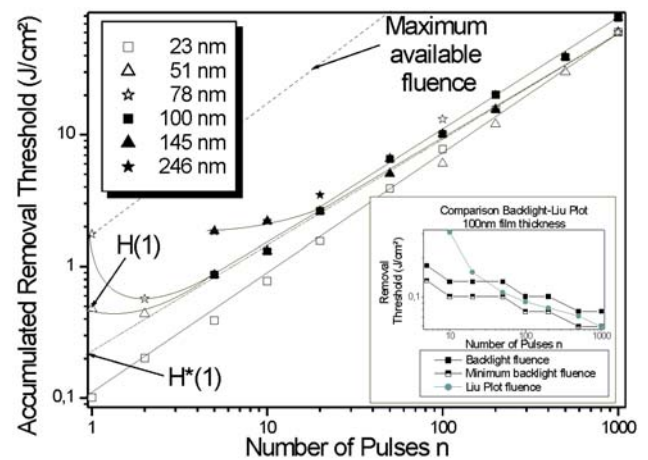
Fig. 6 Accumulated removal threshold determined by backlight microscopy

Fig. 6 depicts accumulated removal thresholds determined by backlight microscopy. Due to the design of the experiments, the fluence can only be determined within discrete levels. This discretization leads to removal thresholds up to 30% higher than those determined by Liu plots. This is caused by the chosen factor of 1.3 for the increase of fluence values. The inset in Fig. 6 depicts the Liu plot removal thresholds, as well as the backlight microcopy thresholds including the minimum value due to the discretization for NiCr films of 100 nm thickness. The removal thresholds determined by backlight microscopy show good agreement with the values determined using the Liu plots for high numbers of pulses. Hence, the threshold determined by both methods can be compared.

The maximum fluence available from the beam source used is depicted as a dashed line. The removal thresholds for more than 50 pulses do not change significantly with the film thickness. The graph for a film thickness of 23 nm shows in the double logarithmic plot linear behavior as expected from the incubation model. The incubation factor has been calculated to be 0.86 according to equation (4). This value is in good agreement with values for the ablation threshold of thin metal films determined by other researchers [7], [8], [12]. The incubation model, which has

been intended for ablation, can be adopted for the removal of 23 nm NiCr film thicknesses.

Film thicknesses above 23 nm and below 100 nm show an unexpected increase in the removal threshold for single pulse ablation. For films with a thickness of 100 nm and above determination of removal thresholds for ablation with one or two pulses was not possible. The maximum achievable fluence of the beam source is lower than the removal threshold of these films.

Calculating the removal threshold for single pulse ablation by regression according to the incubation model will lead to an anticipated removal threshold $H^*(1)$ which is lower than the actual removal threshold $H(1)$. Consequently, the incubation model cannot be applied for the removal of film thicknesses above 23 nm.

The energy penetration depth d_{en} into metals is governed by two characteristic material properties, when using ultra short laser pulses. One is the optical skin depth. The other is the electron-phonon coupling constant g. This constant describes the coupling of the electron and phonon heat equations of the Two Temperature Model (TTM). Low coupling constants g lead to long non-equilibrium times, and therefore high energy diffusion lengths in the electron system. This length is often referred to as the electron diffusion length l_{el} High coupling constants lead to low energy diffusion depths. Typical electron diffusion depths vary from about 50 nm for nickel up to 700 nm for gold. The total energy penetration depth d_{en} is the sum of the optical skin depth δ and the electron diffusion length d_{el}:

$$d_{en} = \delta + d_{el}. \qquad (12)$$

The ablation depth is determined by the depth which ensures the fluence being above the ablation threshold. According to the Beer-Lambert law, the ablation depth can be increased by increasing the applied fluence when machining a certain material. This effect has been reported frequently [12]. But increasing the fluence significantly increases the thermal impact, and leads to melting. Single pulse ablation of film thicknesses clearly above the energy penetration depth is therefore not recommended if precision is required.

The validity of the incubation model for 23 nm thick NiCr films indicates that the energy penetration depth d_{en} is lower or equal to the film thickness. The determined skin depth δ of 12.9 nm indicates the electron diffusion depth d_{el} according to equation (12) to be at least 10.1 nm. The non-proportional increase of the removal threshold and the deviation from the incubation model for the film thickness of 51 nm indicate the energy diffusion depth d_{en} to be smaller than the film thickness. The electron diffusion depth d_{el} according to equation (12) is consequently smaller than 38.1 nm.

The analysis of the Liu plots also allows for calculation of the beam radius. The averaged beam radii for each film thickness calculated with the fit functions are depicted in Fig. 7. All diameters determined in this way are clearly larger than the beam radius of 11.5 µm measured with the MSM. The calculated beam radii show a decrease with growing film thickness, except for the film with 23 nm thickness, which shows a smaller beam radius. The beam radius of this film thickness could be determined for all applied numbers of pulses, as depicted in the inset of Fig. 7.

The calculated beam radii grow with increasing numbers of applied pulses until reaching a constant value. Beam diameters for thicker film could only be determined for more than 10 irradiations and show constant values over the applied number of pulses.
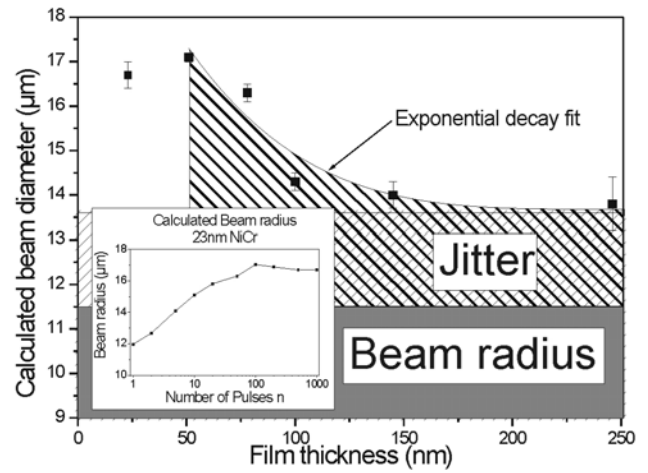
Fig. 7 Calculated beam diameter vs. film thickness

The calculated beam radii being larger than the measured beam radius indicate energy transport lateral to the incident laser radiation. In the following the calculated beam radii for film thicknesses have been fit to an exponential decay

$$\omega_{calc} = (\omega_0 + l_{ind}) + \omega_0 e^{-x/l_{dep}} \qquad (11)$$

with l_{ind} being a film thickness independent energy transportation length, and l_{dep} an energy transportation length coefficient dependent on the film thickness. The reason for the thickness independent transportation length is spatial inaccuracies of the scanner (jitter). The jitter explains the increase of the calculated beam radius with increasing number of pulses for the 23nm NiCr film.

Possible explanations for the film thickness dependent energy transportation coefficient are (i) heat conduction of the electrons, (ii) ballistic electrons or (iii) interaction with the expanding plasma plume. Explanations (i) and (ii) are to be tested by exercising experiments on materials with better known properties, e.g. gold, and explanation (iii) by performing the same experiments in a vacuum, to decrease the interaction of the plasma plume with the remaining material.

Table 2: Fitting results

	Fitting results
l_{ind}	2,1 µm
l_{dep}	51 nm
R^2	0,91

The determined fitting parameters as well as the correlation coefficient R^2 are listed in Table 2. The thickness independent energy transportation length is in the range of the expected jitter. The thickness dependent energy transportation length is slightly larger than the energy penetration length determined by removal threshold analysis.

4. Conclusions

The experiments revealed the optical skin depth of NiCr (80%/20%) to be 12.9 nm ate the wavelength of 532 nm. For the first time the electron diffusion length of NiCr has been identified. It is in the larger than 11.1 nm and smaller than 38.1 nm. The resulting energy penetration depth is larger than 23 nm and smaller than 51 nm. Films with thicknesses above and below the energy penetration depth behave significantly different. Films with a thickness below the energy penetration depth can be completely re-moved by single pulse ablation. Films with thicknesses clearly above the penetration depth can only be removed by multiple pulse ablation. Variation of the film thickness within the interval of 51 nm up to 246 nm does not lead to a significant change of the removal threshold when apply-ing more than 50 pulses. Because variations of the film thickness in industrial production is expected and ablation with too high fluences will cause damage of the substrate, patterning strategies with sequence of 50 or more pulses seem to be a promising way to manufacture NiCr thin film strain gauges.

Beam radii calculated from Liu plots are always larger than the beam radius measured by a beam analysis system. Despite the spatial jitter caused by multiple scan repetitions an additional film thickness dependent coefficient of the beam radius increase has been determined experimentally.

The conclusions enable the mathematical description of the removal of NiCr thin films, and allow consequently for the modeling of the energy input into subjacent layers. In order to transfer the patterning of NiCr thin film strain gauges from the laboratory to fabrication, the modeling of the spot ablations have to be transferred to line ablations. The transfer requires the enhancement of the incubation model by Jee, which covers only static ablation on one spot and should include locally varying fluences as well as an incubation fluence in order to describe the number of af-fecting pulses due to the relative movement between spot and work piece.

Acknowledgments and Appendixes

References

[1] K.H. Imam, P.M. Wild, T.N. Moore, and M. Sayer, Thin Solid Films 515, (2006), 2602.
[2] O.J. Gregory, A.B. Slot, P.S. Amons, and E.E. Cris-man, Surface and Coatings Technology 88, (1996) 79.
[3] J. F. Lei, and H. A. Will,: Sensors and Actuators A 65, (1998), 187.
[4] Lüthje, H.; Biehl, S.; Bandorf, R.: Proc. 6th Int. Conf. Euspen, Volume 1, (2006) 329.
[5] J.M. Liu, Optics Letters Vol. 7, No. 5, 196-198 (1982).
[6] Y. Jee, M.F. Becker and R.M. Walser, J. Opt. Soc. Am. B Vol. 5, No. 3, (1988) 648.
[7] J. Güdde, J. Hohlfeld, J.G. Müller and E. Matthias, Appl. Surface Science 127, (1998) 40.
[8] J. Hohlfeld, S.-S. Wellershoff, J. Güdde, U. Conrad, V. Jähnke and E. Matthias, Chemical Physics 251, (2000) 237.
[9] J. Siegel, K. Ettrich, E. Welsch and E. Matthias, Appl. Phys. 64, (1997) 213
[10] O.Suttmann, M. Gosselin, U.Klug, R. Kling: Proc. Of SPIE 7589, (2010).
[11] S.I. Anisimov, B. Kapeliovich, T. Perel'man: Sov. Phys. JETP 39, (1974), 387.
[12] F. Siegel, U. Klug, R. Kling: Journal of Laser Micro/ Nanoengineering JLMN, Vol. 4 No. 2, (2009), 104.
[13] D. R. Lide: "Handbook of Chemistry and Physics", (CRC Press, 2004), p 12-134-12-142
[14] J.F. Düsing, T. Temme, R. Kling: Proceedings of LANE (2007).
[15] A. Ancona, F. Röser, K. Rademaker, J. Limpert, S. Nolte, A. Tünnermann: Opt. Expr., Vol. 16, Issue 12, (2008), 8958.